

Topological edge states in spin 1 bilinear-biquadratic model

Peng Li

Center for Theoretical Physics, Department of Physics, Sichuan University, Chengdu 610064, China

E-mail: lipeng@scu.edu.cn

Su-Peng Kou

Department of Physics, Beijing Normal University, Beijing 100875, China

E-mail: spkou@bnu.edu.cn

Abstract. The spin 1 bilinear-biquadratic model $H = \sum_{\langle ij \rangle} [\cos \phi \mathbf{S}_i \cdot \mathbf{S}_j + \sin \phi (\mathbf{S}_i \cdot \mathbf{S}_j)^2]$ on square lattice in the region $0 < \phi < \pi/4$ is studied in a fermion representation with a p -wave pairing BCS type mean-field theory. Our results show there may exist a non-trivial gapped spin liquid with time-reversal symmetry spontaneously breaking. This exotic state manifests its topological nature by forming chiral states at the edges. To show it more clear, we set up and solved a ribbon system. We got a gapless dispersion representing the edge modes beneath the bulk modes. The edge modes with nonzero longitudinal momentum ($k_x \neq 0$) convect in opposite directions at the two edges, which leads to a two-fold degeneracy. While the zero longitudinal momentum ($k_x = 0$) modes turn out to be Majorana fermion states. The edge spin correlation functions are found to decay in a power law with the distance increasing. We also calculated the contribution of the edge modes to the specific heat and obtained a linear law at low temperatures.

PACS numbers: 75.10.Kt, 05.30.Fk, 74.20.Fg, 73.43.-f

1. Introduction

In condensed matter physics, the Landau's theories of Fermi liquid and spontaneous symmetry breaking have been the basic principles that account for vast phenomena. For instance, the ground state of the two-dimensional spin S Heisenberg model on a square lattice possesses long range Néel order and the Goldstone modes due to spontaneous spin-rotation symmetry breaking. People have been trying to look for more exotic states in spin systems for a long time. The seminal concept of “resonating valence bond” (RVB) spin liquid state was first proposed by P. W. Anderson [1]. Then, mostly due to its implication of the mechanism of the high temperature superconductivity [2], this field has been flourishing for more than two decades. As a new type of quantum matter, the spin liquid state itself is intriguing since its properties have never been clarified before [3]. Various approaches have shown that quantum spin liquids may exist in two-dimensional (2D) $S = 1/2$ J_1 - J_2 model and the Heisenberg model on the Kagomé lattice. In these models, the quantum spin liquids are accessed (in principle) by appropriate frustrating interactions [4]. However, the nature of the quantum disordered ground state is still under debate. RVB spin liquid state obviously goes beyond the Landau's theories, in which the quasiparticles of Fermi liquid carry both spin and charge quantum numbers. Another exciting field in searching for quantum exotic states beyond the Landau's theory of spontaneous symmetry breaking is the quantum Hall (QH) and fractional quantum Hall (FQH) states. In these states, topological order plays an essential role [5, 6]. In the QH state, a quantized Hall conductance was measured due to the formation of the Landau levels of a 2D electron gas at low temperatures and in strong magnetic field. One of the key features of QH effect is the existence of chiral edge states around the system boundaries. Recently, involving both quantized spin Hall effect [7, 8] and quantized anomalous Hall effect [9], the topological insulator with gapless edge states has been one of the hot issues. The fundamental links between the above two fields have attracted much attention [10]. In this work, we aim to contribute to these interesting topics.

We study the spin 1 bilinear-biquadratic model on square lattice, of which the Hamiltonian is written as

$$H = \sum_{\langle ij \rangle} [\cos \phi \mathbf{S}_i \cdot \mathbf{S}_j + \sin \phi (\mathbf{S}_i \cdot \mathbf{S}_j)^2], \quad (1)$$

where \mathbf{S}_i is a spin 1 operator. Its semiclassical version ($S \rightarrow \infty$) on a bipartite lattice exhibits four ordered phases that are exactly divided by four $SU(3)$ symmetric points at the model parameters, $\phi = \phi_0 = \pi/4, \pm\pi/2, -3\pi/4$ [11, 12]. They are phases with ferromagnetic (FM), antiferromagnetic (AFM), ferroquadrupolar (FQ), and antiferroquadrupolar (AFQ) orders respectively. Whether these classically well-understood phases are stable in the quantum case or how the quantum model behaves constitutes the interesting topics of current researches. In one dimension (1D), many aspects have been revealed by extensive exploration [13, 14, 15, 16, 17, 18, 19, 20, 21, 22, 23, 24, 25]. While in two dimensions (2D), a complete understanding of the system is still being anticipated. On triangular lattice, many methods have revealed

that the region $\pi/4 < \phi \leq \pi/2$ exhibits an AFQ order [26, 27, 28]. On the honeycomb lattice, a tensor renormalization group method showed the AFQ order in the region $\pi/4 < \phi \leq \pi/2$ is destroyed by pure quantum fluctuations and there is a transition from the plaquette order to the AFM order [29]. A recent work proposed that a three-sublattice order exists in the SU(3) point $\phi_0 = \pi/4$ [30]. The quantum Monte Carlo simulation [31] found the AFM phase is stable in the region $-\pi/2 < \phi \leq 0$ on a square lattice. While in the region of $0 < \phi < \pi/4$, there lacks evidence on whether the AFM order can survive or not.

In this paper, we show that a novel type of topological spin liquid might exist on a square lattice in the region $0 < \phi < \pi/4$, in which a topological edge state circulates around the boundary of the system. Time-reversal symmetry is broken spontaneously for this non-trivial gapped spin liquid. In a fermion representation we found that the 2D spin liquid can be described very well by the (projected) spinless p -wave pairing Bardeen-Cooper-Schrieffer (BCS)-type Hamiltonian. We obtained the gapless dispersion of the edge modes. For a nonzero longitudinal momentum $k_x \neq 0$, one edge mode splits into two half modes that can exist individually, which could be termed \mathcal{L} (left) and \mathcal{R} (right) chiral modes, respectively. While for $k_x = 0$, zero edge modes emerge, which turn out to be Majorana fermion states [32, 33].

The paper is organized as follows. In Section II a brief introduction of the fermion representation is presented. In Section III the mean-field theory is introduced and the solutions of a gapped chiral spin liquid are obtained. Then the corresponding edge state of a ribbon system is explored in Section IV. And a summary is made in Section V.

2. Fermion representation with hard-core constraint

Firstly we introduce a fermion representation for quantum spin 1. Each spin has three eigenstates $|m_j\rangle$ of S_j^z with the eigenvalues $m_j = -1, 0, +1$. We introduce three fermionic operators to generate three independent states ($\mathbf{i} = \sqrt{-1}$),

$$f_{i,1}^\dagger |0\rangle = \frac{\mathbf{i}}{\sqrt{2}} (|m_i = -1\rangle + |m_i = 1\rangle), \quad (2)$$

$$f_{i,2}^\dagger |0\rangle = |m_i = 0\rangle, \quad (3)$$

$$f_{i,3}^\dagger |0\rangle = \frac{1}{\sqrt{2}} (|m_i = -1\rangle - |m_i = 1\rangle). \quad (4)$$

In terms of f operators, the spin operators can be expressed as

$$S_i^x = \mathbf{i}(f_{i,2}^\dagger f_{i,1} - f_{i,1}^\dagger f_{i,2}), \quad (5)$$

$$S_i^y = \mathbf{i}(f_{i,3}^\dagger f_{i,2} - f_{i,2}^\dagger f_{i,3}), \quad (6)$$

$$S_i^z = \mathbf{i}(f_{i,1}^\dagger f_{i,3} - f_{i,3}^\dagger f_{i,1}). \quad (7)$$

To restore the Hilbert space of spin 1, the hard-core constraint at each site must be imposed,

$$\sum_{\mu=1}^3 f_{i,\mu}^\dagger f_{i,\mu} = 1. \quad (8)$$

In this way the Hamiltonian Eq. (1) is mapped to a frustrated SU(3) fermion model [34]

$$H = -J_1 \sum_{\langle ij \rangle} : F_{ji}^\dagger F_{ji} : - J_2 \sum_{\langle ij \rangle} B_{ji}^\dagger B_{ji} + \sum_i \lambda_i \left(\sum_\mu f_{i,\mu}^\dagger f_{i,\mu} - 1 \right), \quad (9)$$

where $J_1 = \cos \phi > 0$, $J_2 = \cos \phi - \sin \phi > 0$, $::$ denotes normal ordering of operators, λ_i are the Lagrangian multipliers, and the bond operators are defined as

$$F_{ji} = \sum_{\mu=1,2,3} f_{j,\mu}^\dagger f_{i,\mu}, \quad B_{ji} = \sum_{\mu=1,2,3} f_{j,\mu} f_{i,\mu}. \quad (10)$$

A similar fermion representation could be found in a recent work [35].

3. Gapped spin liquid with time-reversal symmetry breaking

3.1. Bond-operator mean-field theory

To find the ground state properties of this spin 1 system, we take the mean field approximation by introducing two order parameters for the bond operators B_{ji} and F_{ji} ,

$$\langle F_{i+x,i} \rangle = \langle F_{i+y,i} \rangle = F, \quad (11)$$

$$-i \langle B_{i+x,i} \rangle = B_x = B e^{i\eta_x}, \quad -i \langle B_{i+y,i} \rangle = B_y = B e^{i\eta_y}, \quad (12)$$

where F , B , η_x , and η_y are real and to be determined self-consistently. Here we have taken a uniform phase factor in F , which turns out to be negligible when the mean-field equations are established. Two phase factors are kept for B field, and we will see the final results only rely on the phase difference $\Delta\eta = \eta_y - \eta_x$. Under these prescription, the effective Hamiltonian reads

$$H_{eff} = \sum_{i,\mu} \lambda f_{i,\mu}^\dagger f_{i,\mu} + \sum_{\langle ij \rangle, \mu} \left(f_{j,\mu}^\dagger T_{ji} f_{i,\mu} + h.c. \right) + \sum_{\langle ij \rangle, \mu} \left(f_{j,\mu}^\dagger P_{ji} f_{i,\mu}^\dagger + h.c. \right) - \lambda N_\Lambda + 2N_\Lambda J_1 F^2 + 2N_\Lambda J_2 B^2, \quad (13)$$

where $T_{ji} = -2J_1 \langle F_{ji} \rangle$, $P_{ji} = -2J_2 \langle B_{ji} \rangle$, and N_Λ is the total number of lattice sites. The hard-core constraint shall be imposed on an average level by minimizing the free energy. After performing the Fourier transformation, we arrive at a complex p -wave-like pairing of independent flavor of fermions [36],

$$H_{eff} = \frac{1}{2} \sum_{\mathbf{k}, \mu} \Phi_\mu^\dagger(\mathbf{k}) M(\mathbf{k}) \Phi_\mu(\mathbf{k}) + \varepsilon_0, \quad (14)$$

$$\varepsilon_0 = \frac{1}{2} \lambda N_\Lambda + 2N_\Lambda J_1 F^2 + 2N_\Lambda J_2 B^2. \quad (15)$$

where the sum of momentum \mathbf{k} is carried out in the first Brillouin zone ($1^{st} BZ$), the spinor $\Phi_\mu^\dagger(\mathbf{k}) = \left(f_{\mathbf{k},\mu}^\dagger, f_{-\mathbf{k},\mu} \right)$, the 2×2 Hermitian matrix

$$M(\mathbf{k}) = \mathbf{d}(\mathbf{k}) \cdot \boldsymbol{\sigma} \quad (16)$$

with the Pauli matrices $\sigma = (\sigma_x, \sigma_y, \sigma_z)$ and

$$\mathbf{d}(\mathbf{k}) = (d_x(\mathbf{k}), d_y(\mathbf{k}), d_z(\mathbf{k})), \quad (17)$$

$$d_x(\mathbf{k}) = 2J_2B(\cos \eta_x \sin k_x + \cos \eta_y \sin k_y), \quad (18)$$

$$d_y(\mathbf{k}) = 2J_2B(\sin \eta_x \sin k_x + \sin \eta_y \sin k_y), \quad (19)$$

$$d_z(\mathbf{k}) = \lambda - 2J_1F(\cos k_x + \cos k_y). \quad (20)$$

The Lagrangian multiplier λ_i is taken to be site-independent, $\lambda_i = \lambda$, which can also be regarded as a mean field. N_Λ is the total number of lattice sites, and in fact we have defined in this way a mean field Hamiltonian that is similar to the 2D Kiteav model for the $p + ip$ superconductors for spinless fermions [33, 37]. But the hard core constraint in Eq. (8) may make it different. By performing the Bogoliubov transformation, one can diagonalize the Hamiltonian as

$$H_{eff} = \frac{1}{2} \sum_{\mathbf{k}, \mu} \Psi_\mu^\dagger(\mathbf{k}) P(\mathbf{k}) \Psi_\mu(\mathbf{k}) + \varepsilon_0, \quad (21)$$

where $P(\mathbf{k}) = \omega(\mathbf{k})\sigma_z$, $\Psi_\mu^\dagger(\mathbf{k}) = (\gamma_{\mathbf{k}, \mu}^\dagger, \gamma_{-\mathbf{k}, \mu})$ with $\gamma_{\mathbf{k}, \mu} = u_{\mathbf{k}} f_{\mathbf{k}, \mu} - v_{\mathbf{k}} f_{-\mathbf{k}, \mu}^\dagger$, where the coefficients satisfy

$$|u_{\mathbf{k}}|^2 = \frac{1}{2} \left[1 + \frac{d_z(\mathbf{k})}{\omega(\mathbf{k})} \right], \quad (22)$$

$$|v_{\mathbf{k}}|^2 = \frac{1}{2} \left[1 - \frac{d_z(\mathbf{k})}{\omega(\mathbf{k})} \right], \quad (23)$$

$$2u_{\mathbf{k}}^* v_{\mathbf{k}} = \frac{d_x(\mathbf{k}) + i d_y(\mathbf{k})}{\omega(\mathbf{k})}. \quad (24)$$

If one chooses a real and even $v_{\mathbf{k}}$ ($v_{\mathbf{k}}^* = v_{\mathbf{k}}$), then $u_{\mathbf{k}}$ is complex and odd, and vice versa. The spectrum is

$$\omega(\mathbf{k}) = |\mathbf{d}(\mathbf{k})| = \sqrt{d_x^2(\mathbf{k}) + d_y^2(\mathbf{k}) + d_z^2(\mathbf{k})}. \quad (25)$$

The free energy can be worked out as

$$F = -\frac{3}{\beta} \sum_{\mathbf{k}} \ln(1 + e^{-\beta\omega(\mathbf{k})}) + E_0, \quad (26)$$

where $\beta = \frac{1}{k_B T}$ and the ground state energy is

$$E_0 = -\frac{3}{2} \sum_{\mathbf{k}} \omega(\mathbf{k}) + \varepsilon_0. \quad (27)$$

By optimizing the free energy with respect to the mean fields, one obtains the mean-field equations as the follows,

$$\frac{1}{3} = \frac{1}{N_\Lambda} \sum_{\mathbf{k}} \frac{d_z(\mathbf{k})}{\omega(\mathbf{k})} \tanh \frac{\beta\omega(\mathbf{k})}{2}, \quad (28)$$

$$F = \frac{3}{2} \frac{1}{N_\Lambda} \sum_{\mathbf{k}} \frac{-d_z(\mathbf{k}) (\cos k_x + \cos k_y)}{2\omega(\mathbf{k})} \tanh \frac{\beta\omega(\mathbf{k})}{2}, \quad (29)$$

$$B(\cos \eta_x + \cos \eta_y) = \frac{3}{2} \frac{1}{N_\Lambda} \sum_{\mathbf{k}} \frac{d_x(\mathbf{k}) (\sin k_x + \sin k_y)}{\omega(\mathbf{k})} \tanh \frac{\beta\omega(\mathbf{k})}{2}, \quad (30)$$

$$B(\sin \eta_x + \sin \eta_y) = \frac{3}{2} \frac{1}{N_\Lambda} \sum_{\mathbf{k}} \frac{d_y(\mathbf{k}) (\sin k_x + \sin k_y)}{\omega(\mathbf{k})} \tanh \frac{\beta\omega(\mathbf{k})}{2}. \quad (31)$$

All the mean fields can be determined by solving the set of mean-field equations self-consistently. It is remarkable that all dispersions for quasi-particles are three-fold degenerate at the mean field level. Coexistence of non-zero solutions for both mean fields F and B affirms the meaningful bond operator decomposition scheme in Eq. (9)-(10). Notice that the spectrum Eq. (25) is a function of the phase difference $|\Delta\eta| = |\eta_y - \eta_x|$, we can also take $|\Delta\eta|$ as the optimizing parameter. It is clear to see that the effective Hamiltonian Eq. (14) preserves the time-reversal symmetry when $|\Delta\eta| = 0$ [34], and does not when $|\Delta\eta| \neq 0$. The equations are solved at zero temperature to reveal the ground state properties. The non-zero solution of mean fields λ , F and B for several choices of phase difference $|\Delta\eta|$ are illustrated in Figure 1. At zero temperature, one can get a simple form for the ground state energy

$$E_0 = -2N_\Lambda J_1 F^2 - 2N_\Lambda J_2 B^2, \quad (32)$$

where λ is cancelled due to the substitution of the mean-field equations Eq. (28)-(31) in Eq. (27). The numerical solution for the ground state energy E_0 and the gap of energy spectrum, $\Delta_{gap} = \min(\omega(\mathbf{k}))$, are illustrated in Figure 2. We found that the lowest energy state can be reached by choosing the phase difference $|\Delta\eta| = \pi/2$. This solution is a p -wave paired gapped spin liquid and breaks the time-reversal symmetry. The gapped spin liquid revealed here can be classified by the Z_2 invariant [38]. And by the Z_2 invariant in the topological spin liquid state, we find a special fermion parity pattern at high symmetry points in momentum space: even fermion parity at $\mathbf{k} = (\pi, \pi)$, $\mathbf{k} = (0, \pi)$, and $\mathbf{k} = (\pi, 0)$ and odd fermion parity at $\mathbf{k} = (0, 0)$ (please see detailed calculations in Appendix). The physical regime of the spin liquid should not exceed the Heisenberg point $\phi_H = 0$, because the regime with $-\pi/2 < \phi \leq \phi_H = 0$ exhibits an antiferromagnetic order [31]. The meaningful numerical solutions with nonzero F and B for $|\Delta\eta| = \pi/2$ ceases near $\phi \gtrsim -0.08$ (see Figure 2), a little less than $\phi_H = 0$. The discrepancy can be ascribed to the crudeness of the mean-field theory. At the SU(3) point $\phi_0 = \pi/4$ [30], our result shows that the gap closes along the loop line $\mathbf{k}^* = (k_x^*, k_y^*) : \cos k_x^* + \cos k_y^* = 1/A$ with $A = 2.412513447$, where the spectrum behaves linearly as $\omega(\mathbf{k}) \sim c(\mathbf{k}^*) |\mathbf{k} - \mathbf{k}^*|$ with anisotropic velocity $c(\mathbf{k}^*)$. The gaplessness on the loop line does not imply any order, so we get a gapless spin liquid that is highly degenerate in thermodynamic limit.

3.2. Ground state and the Chern number

The p -wave paired ground state of the bulk system reads [36]

$$|\Omega_0\rangle = \prod_{\mathbf{k}, \mu}' \left(u_{\mathbf{k}} + v_{\mathbf{k}} f_{\mathbf{k}, \mu}^\dagger f_{-\mathbf{k}, \mu}^\dagger \right) |0\rangle, \quad (33)$$

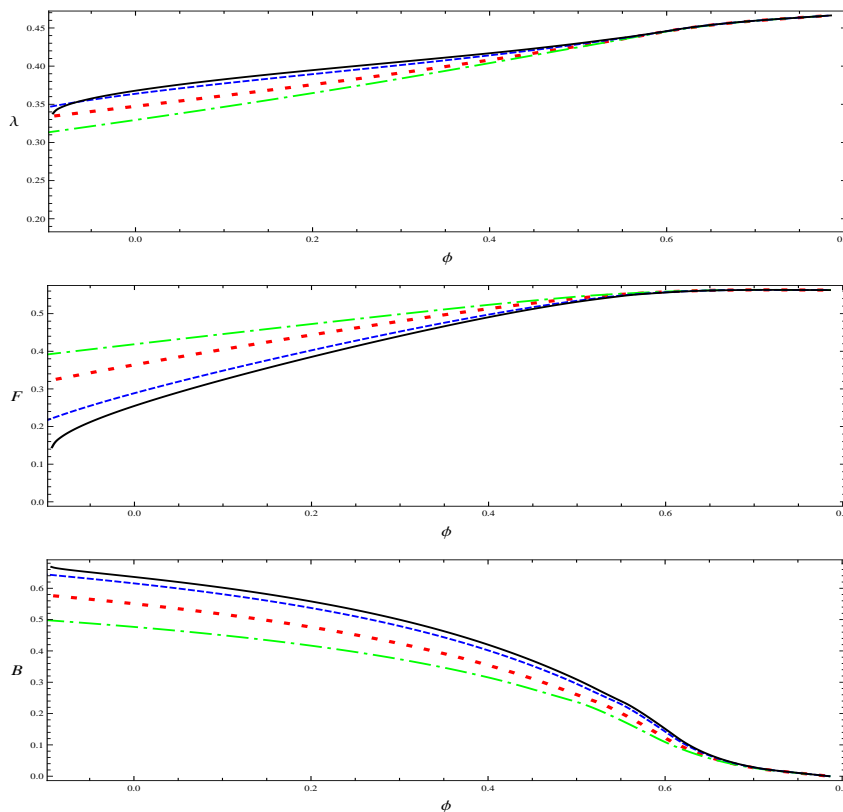


Figure 1. (Color online) Numerical solution for the Lagrangian multiplier λ and the mean fields F and B . The lines for several selected phase differences are: $|\Delta\eta| = |\eta_x - \eta_y| = \pi/2$, black solid line; $\pi/3$, blue dashed line; $\pi/6$, red dotted line; 0, green dot-dashed line. Please see more details in the text.

where the prime on the product indicates that each distinct pair $(\mathbf{k}, -\mathbf{k})$ is to be taken once. This ground state exhibits a non-trivial topological property that can be signified by the Chern number of the spinless SU(3) fermions. For each flavor of spinless fermions, the Chern number is defined by [36, 39]

$$C = \frac{1}{4\pi} \int_{\Omega} d^2k [\mathbf{n}(\mathbf{k}) \cdot \partial_{k_x} \mathbf{n}(\mathbf{k}) \times \partial_{k_y} \mathbf{n}(\mathbf{k})] \quad (34)$$

where Ω means the volume of the first Brillouin zone, $\mathbf{n}(\mathbf{k})$ is defined as $\mathbf{n}(\mathbf{k}) = \frac{\mathbf{d}(\mathbf{k})}{|\mathbf{d}(\mathbf{k})|}$. By substituting Eq. (17) in Eq. (34), we get

$$C = \frac{\sin(\Delta\eta)}{4\pi} \left(\frac{2J_2 B}{\lambda} \right)^2 \int_{\Omega} d^2k \frac{[\frac{2J_1 F}{\lambda} (\cos k_x + \cos k_y) - \cos k_x \cos k_y]}{(\omega(\mathbf{k})/\lambda)^3}, \quad (35)$$

And by substituting the numerical mean-field solutions at zero temperature in, we obtain the simplified result,

$$C = \pm 1, \quad (36)$$

for $0 < \phi < \pi/4$. Thus the total Chern number of this topological state is $C = \pm 3$ due to symmetry for the fermions of different flavors. The bulk system's nontrivial ground state can be labeled by this Chern number.

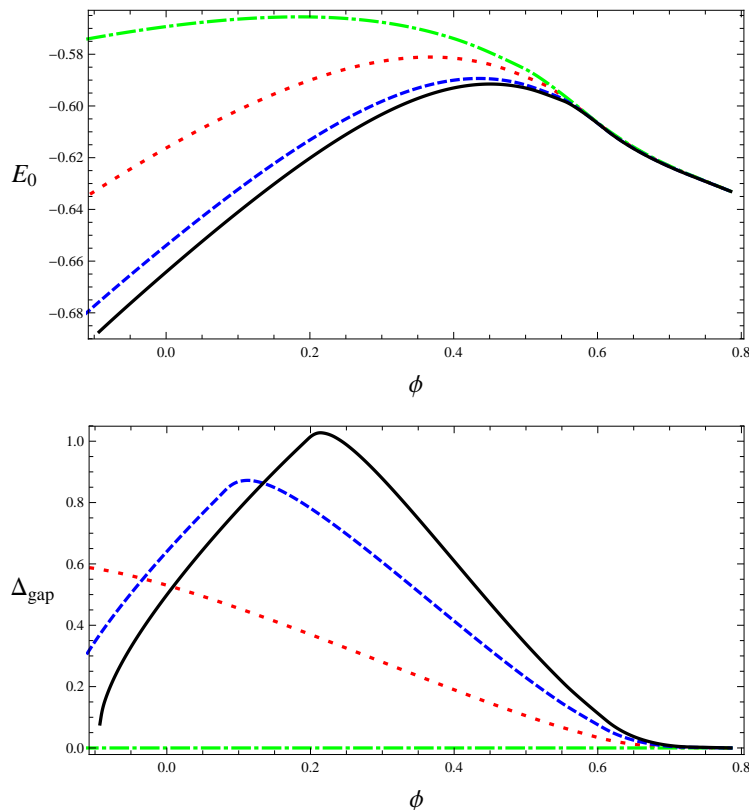


Figure 2. (Color online) Upper: the ground state energy E_0 ; lower: the gap of energy spectrum, $\Delta_{\text{gap}} = \min(\omega(\mathbf{k}))$. The line types are the same as the ones described in Figure 1.

4. Spin edge states

4.1. Edge modes of the ribbon system

To demonstrate the spin edge states explicitly, we set up a ribbon (or ladders) system with a pair of open edges in \hat{y} direction and keep periodic boundary condition along \hat{x} axis (Figure 3). Noticing that k_x is still a good quantum number, we start with an Hamiltonian with L_{max} legs,

$$H'_{eff} = \sum_{k_x \geq 0, \mu} \Phi_\mu^\dagger(k_x) M(k_x) \Phi_\mu(k_x) + \varepsilon_0, \quad (37)$$

$$\Phi_\mu^\dagger(k_x) = \left(f_{(k_x, 1), \mu}^\dagger, \dots, f_{(k_x, L_{\text{max}}), \mu}^\dagger; f_{(-k_x, 1), \mu}, \dots, f_{(-k_x, L_{\text{max}}), \mu} \right), \quad (38)$$

where we have parsed the zero momentum states in the first term and restricted the sum to the positive values of momentum. The matrix $M(k_x)$ are too large to be presented here. One can easily solve the Hamiltonian numerically. The resulting diagonalized Hamiltonian could be written in the form

$$H'_{eff} = \sum_{k_x \geq 0, \mu} \Psi_\mu^\dagger(k_x) P(k_x) \Psi_\mu(k_x) + \varepsilon_0, \quad (39)$$

$$P(k_x) = \text{dia} \left[\omega_{(k_x, 1)}, \dots, \omega_{(k_x, L_{\text{max}})}; -\omega_{(k_x, 1)}, \dots, -\omega_{(k_x, L_{\text{max}})} \right], \quad (\omega_{(k_x, i)} \geq 0) \quad (40)$$

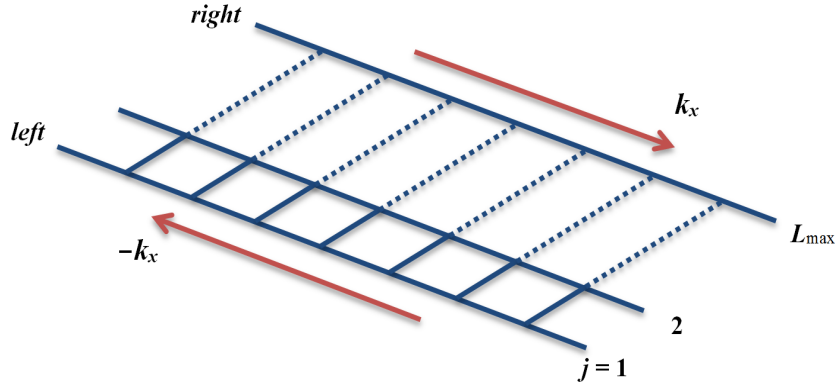


Figure 3. (Color online) The ribbon system with open boundaries in \hat{y} direction. The edge modes at the two edges convect in opposite directions.

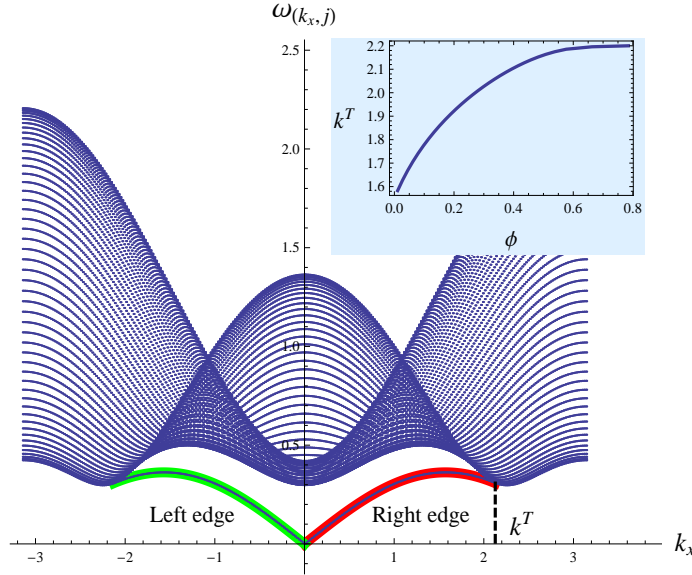


Figure 4. (Color online) Numerical solutions of the spectra of the ribbon for the selected model parameter $\phi = 0.435847$. The system's size is $L_{\max} = 50$. The lowest thick line denotes the edge spectrum Eq. (46). Notice the gauge choice $\Delta\eta = \pi/2$ is taken here, so we have right modes for $k_x > 0$ and left modes for $k_x < 0$. The inset shows the upper value k^T for the edge states as a function of model parameter ϕ .

$$\Psi_{\mu}^{\dagger}(k_x) = \left(\gamma_{(k_x,1),\mu}^{\dagger}, \dots, \gamma_{(k_x,L_{\max}),\mu}^{\dagger}; \gamma_{(-k_x,1),\mu}, \dots, \gamma_{(-k_x,L_{\max}),\mu} \right), \quad (41)$$

or a further simplified one

$$H'_{eff} = \sum_{k_x \geq 0, \mu, i} \omega_{(k_x, i)} \left[\gamma_{(k_x, i), \mu}^{\dagger} \gamma_{(k_x, i), \mu} + \gamma_{(-k_x, i), \mu}^{\dagger} \gamma_{(-k_x, i), \mu} \right] - \sum_{k_x \geq 0, \mu, i} \omega_{(k_x, i)} + \varepsilon_0. \quad (42)$$

We choose the canonical operator $\gamma_{(k_x,1),\mu}^{\dagger}$ (with subscript $i = 1$) to denote the edge excitations above the ground state and $\omega_{(k_x,1)}$ the edge excitation energy. The rest modes are bulk modes. The new ground state $|\Omega'_0\rangle$ is quite different from that in Eq.

(33). $|\Omega'_0\rangle$ itself contains the chirality of the edges and should satisfy the condition

$$\gamma_{(k_x,i),\mu} |\Omega'_0\rangle = 0, \forall k_x, i, \mu. \quad (43)$$

We will specify the ground state numerically later when evaluating some quantities. The lowest energy mode for each k_x could be collected as

$$H'_{lowest} = \sum_{k_x \geq 0, \mu} \omega_{(k_x,1)} \left[\gamma_{(k_x,1),\mu}^\dagger \gamma_{(k_x,1),\mu} + \gamma_{(-k_x,1),\mu}^\dagger \gamma_{(-k_x,1),\mu} \right]. \quad (44)$$

It seems that this effective Hamiltonian denotes the edge states. However, this is not necessarily the case. The lowest spectrum is a piecewise function

$$\omega_{(k_x,1)} = \begin{cases} 2J_2B |\sin k_x|, & (|k_x| \leq k^T); \\ \sqrt{[\lambda - 2J_1F(1 + \cos k_x)]^2 + 4J_2^2B^2 \sin^2 k_x}, & (|k_x| > k^T), \end{cases} \quad (45)$$

where $k^T = \arccos(\lambda/2J_1F - 1)$ denotes a transition point. At this transition point, both $\omega_{(k_x,1)}$ and its first-order derivative are continuous, but its second-order derivative is discontinuous. One would find that only the first piece is the edge mode spectrum, i.e. the edge mode spectrum ceases at k^T and reads

$$\omega_{(k_x,1)}^{edge} = 2J_2B |\sin k_x|, (-k^T \leq k_x \leq k^T), \quad (46)$$

While the second piece is still a bulk mode spectrum. These conclusions are testified by our numerical solutions.

4.2. Numerical solution of the chiral edge states and zero mode Majorana fermion states

Now we discuss some more details about our numerical results. From the numerical results, we confirm that the edge modes are well localized at the edges. In practice, the solutions with $\Delta\eta = \pi/2$ and $\Delta\eta = -\pi/2$ are degenerate, but have opposite chirality. So we only demonstrate the solution for $\Delta\eta = \pi/2$ and $\phi = 0.435847$ in Figure 4. For $0 < k_x \leq k^T$, we find the edge mode $\gamma_{(-k_x,1),\mu}^\dagger$ localized at the left edge and $\gamma_{(k_x,1),\mu}^\dagger$ at the right edge. Thus we may call them left (\mathcal{L}) and right (\mathcal{R}) chiral modes respectively,

$$\mathcal{L}_\mu(-k_x) \equiv \gamma_{(-k_x,1),\mu} = \sum_{j=1}^{L_{\max}} \left[U_{(-k_x,j)} f_{(k_x,j),\mu} + V_{(-k_x,j)} f_{(-k_x,j),\mu}^\dagger \right], \quad (47)$$

$$\mathcal{R}_\mu(k_x) \equiv \gamma_{(k_x,1),\mu} = \sum_{j=1}^{L_{\max}} \left[U_{(k_x,j)} f_{(k_x,j),\mu} + V_{(k_x,j)} f_{(-k_x,j),\mu}^\dagger \right], \quad (48)$$

where the coefficients U and V are real (as is contrast to the coefficients $u_{\mathbf{k}}$ and $v_{\mathbf{k}}$ for the periodic boundary in previous section) and depicted in Figure 5(a) and (b). With the increasing size of the system, the zero-momentum edge excitation $\omega_{(0,1)}^{edge}$ goes to zero rapidly. Beyond $L_{\max} = 50$, its energy value is so small that one can hardly discern it from the machine precision. We may denote the zero modes as

$$\mathcal{E}_\mu \equiv \gamma_{(0,1),\mu} = \sum_{j=1}^{L_{\max}} \left[U_{(0,j)} f_{(0,j),\mu} + V_{(0,j)} f_{(0,j),\mu}^\dagger \right], \quad (49)$$

where the real coefficients are depicted in Figure 5(c). We see this zero modes manifest itself at both edges. It is in fact a Majorana fermion state [32], since the mode contributes zero energy to the system and can be rewritten as

$$\mathcal{E}_\mu^\dagger \mathcal{E}_\mu = 1 - 2\mathbf{i} \mathcal{M}_\mu^\mathcal{L} \mathcal{M}_\mu^\mathcal{R} \quad (50)$$

with two Majorana fermions

$$\mathcal{M}_\mu^\mathcal{L} = \sum_{j=1}^{L_{\max}} \frac{U_{(0,j)} - V_{(0,j)}}{2} \left(-\mathbf{i} f_{(0,j),\mu} + \mathbf{i} f_{(0,j),\mu}^\dagger \right), \quad (51)$$

$$\mathcal{M}_\mu^\mathcal{R} = \sum_{j=1}^{L_{\max}} \frac{U_{(0,j)} + V_{(0,j)}}{2} \left(f_{(0,j),\mu} + f_{(0,j),\mu}^\dagger \right), \quad (52)$$

localizing at the two opposite edges. All of the above coefficients satisfy the relations numerically for large enough L_{\max} ($k_x \geq 0$)

$$\sum_{j=1}^{L_{\max}} [U_{(\mp k_x, j)}^2 + V_{(\mp k_x, j)}^2] = 1, \quad (53)$$

$$U_{(k_x, j)} = V_{(k_x, j)}, U_{(-k_x, j)} = -V_{(-k_x, j)}, \quad (54)$$

$$U_{(-k_x, j)} = -U_{(k_x, L_{\max}-j+1)}, V_{(-k_x, j)} = V_{(-k_x, L_{\max}-j+1)}, \quad (55)$$

$$U_{(-k_x, j)} U_{(k_x, j)} = V_{(-k_x, j)} V_{(k_x, j)} = 0. \quad (56)$$

But notice each mode possess a U(1) symmetry, so that the values may be changed according to the symmetry transformation.

4.3. Edge spin correlation functions

Although the edge states of the ribbon are clear to see in the fermion representation, it is still illusive from the point of view of the spin language. In order to show the properties of the spin edge state, we measure the spin correlations and thermodynamic quantities, such as the specific heat, contributed by the edge.

It is well-known a gapped spin system exhibits an exponentially decaying spin correlation in the bulk. Of all the spin correlations for the ribbon system, the one at the edge is of our great interest. We choose the right edge of the ribbon (Figure 3) to measure the spin correlations in the ground state,

$$C_{edge}^{zz}(i, i+r) \equiv C_{edge}^{zz}(r) = \langle S_{(i, L_{\max})}^z S_{(i+r, L_{\max})}^z \rangle. \quad (57)$$

Now we need to find out the the ground state $|\Omega'_0\rangle$. The edge modes in H'_{edge} could be singled out and serve as a quasi-1D effective Hamiltonian,

$$H'_{eff} = H'_{bulk} + H'_{edge}, \quad (58)$$

$$H'_{edge} = \sum_{0 \leq k_x \leq k_T, \mu} \omega_{(k_x, 1)}^{edge} \left[\gamma_{(k_x, 1), \mu}^\dagger \gamma_{(k_x, 1), \mu} + \gamma_{(-k_x, 1), \mu}^\dagger \gamma_{(-k_x, 1), \mu} \right], \quad (59)$$

which could be utilized to evaluate quantities along the edges. Near $k_x \sim 0$, the edge modes behave linearly $\omega_{(k_x, 1)}^{edge} \sim 2J_2 B |k_x|$ [33](please see the lowest thick line in Figure

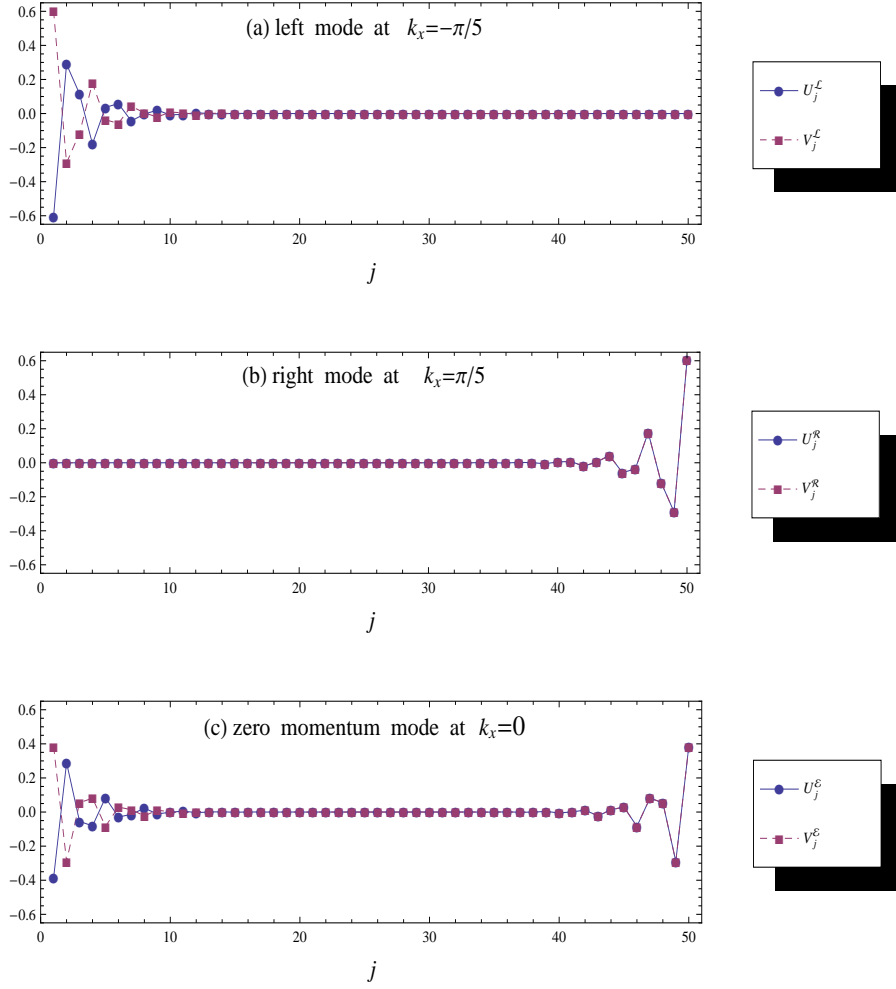


Figure 5. Visualization of the edge modes in fermion representation on a ribbon with width $L_{\max} = 50$ ($1 \leq j \leq L_{\max}$): (a) the left modes at $k_x = -\pi/5$, (b) the right mode at $k_x = \pi/5$ and (c) the zero momentum mode at $k_x = 0$. The model parameter $\phi = 0.435847$ and gauge choice $\Delta\eta = \pi/2$.

4). Since the bulk and edge modes are independent, one can write the ground state in a separable form

$$|\Omega'_0\rangle = |\Omega'_{0,bulk}\rangle \otimes |\Omega'_{0,edge}\rangle, \quad (60)$$

where $|\Omega'_{0,bulk}\rangle$ and $|\Omega'_{0,edge}\rangle$ are the lowest energy states of H'_{bulk} and H'_{edge} respectively. We have

$$|\Omega'_{0,edge}\rangle = \prod_{0 \leq k_x \leq k^T, j, \mu} \left[U_{(k_x, j)} - V_{(k_x, j)} f_{(k_x, j), \mu}^\dagger f_{(-k_x, j), \mu}^\dagger \right] |0\rangle, \quad (61)$$

where the prime on the product indicates that each distinct pair $(k_x, -k_x)$ is to be taken once. One can easily verify that $\gamma_{(\mp k_x, 1), \mu} |\Omega'_{0,edge}\rangle = 0$. Since we are concerning the quantities along the edge, the edge correlation function Eq. (57) can be evaluated

approximately just by $|\Omega'_{0,edge}\rangle$. At first, one can work out

$$\begin{aligned} \left\langle f_{(k_x, L_{\max}), \mu}^\dagger f_{(-k_x, L_{\max}), \mu}^\dagger \right\rangle &= -U_{(k_x, L_{\max})} V_{(k_x, L_{\max})}, \\ \left\langle f_{(k_x, L_{\max}), \mu}^\dagger f_{(k_x, L_{\max}), \mu} \right\rangle &= V_{(k_x, L_{\max})}^2. \end{aligned} \quad (62)$$

Then the correlation function is deduced as

$$\begin{aligned} C_{edge}^{zz}(r) &= 2 \left| \frac{1}{N_\Lambda} \sum_{0 \leq k_x \leq k^T} e^{i k_x r} \left\langle f_{(k_x, L_{\max}), \mu}^\dagger f_{(-k_x, L_{\max}), \mu}^\dagger \right\rangle \right|^2 \\ &\quad + 2 \left| \frac{1}{N_\Lambda} \sum_{0 \leq k_x \leq k^T} e^{i k_x r} \left\langle f_{(k_x, L_{\max}), \mu}^\dagger f_{(k_x, L_{\max}), \mu} \right\rangle \right|^2 \\ &= 2 \left| \frac{1}{N_\Lambda} \sum_{0 \leq k_x \leq k^T} e^{i k_x r} U_{(k_x, L_{\max})} V_{(k_x, L_{\max})} \right|^2 + 2 \left| \frac{1}{N_\Lambda} \sum_{0 \leq k_x \leq k^T} e^{i k_x r} V_{(k_x, L_{\max})}^2 \right|^2 \end{aligned} \quad (63)$$

The results show a general power law

$$C_{edge}^{zz}(r) \approx \frac{\alpha}{r^\delta}. \quad (64)$$

In practice, we fit the numerical data by the formula

$$\ln C_{edge}^{zz}(r) \approx \ln \alpha - \delta \ln r \quad (65)$$

instead. At the model parameter $\phi = 0.435847$, we obtain $\alpha \approx 0.0156407$ and $\delta \approx 2.174343$ (see Figure 6(a)). For other model parameters, the results are not much different (Figure 6(b) and (c)). So we see that the edge spin correlations decay like a power law along the edge and exclude the possibility of exponential decay behavior in the main region of model parameters.

4.4. Specific heat contributed by the edge modes

Now we turn to the specific heat. At low temperatures, the bulk states contribute little to the specific heat due to the existence of bulk gap, while the gapless edge modes give the main contribution. By adopting Eq. (58) as the effective Hamiltonian, one can worked out the contribution of the edge modes to the specific heat that behaves linearly in temperature T ,

$$\frac{C_V}{N_\Lambda k_B} = \int_0^{E_m} \left(\frac{E}{2k_B T} \right)^2 \cosh^{-2} \left(\frac{E}{2k_B T} \right) \rho(E) dE \approx \frac{\pi k_B}{8J_2 B} T, \quad (66)$$

where we have released the upper limit of the integral for simplicity ($E_m \rightarrow \infty$) and the density of states is

$$\rho(E) = \frac{1}{N_\Lambda} \sum_{k_x, \mu} \delta(E - \omega_{(k_x, 1)}) \approx \frac{3}{2\pi J_2 B}. \quad (67)$$

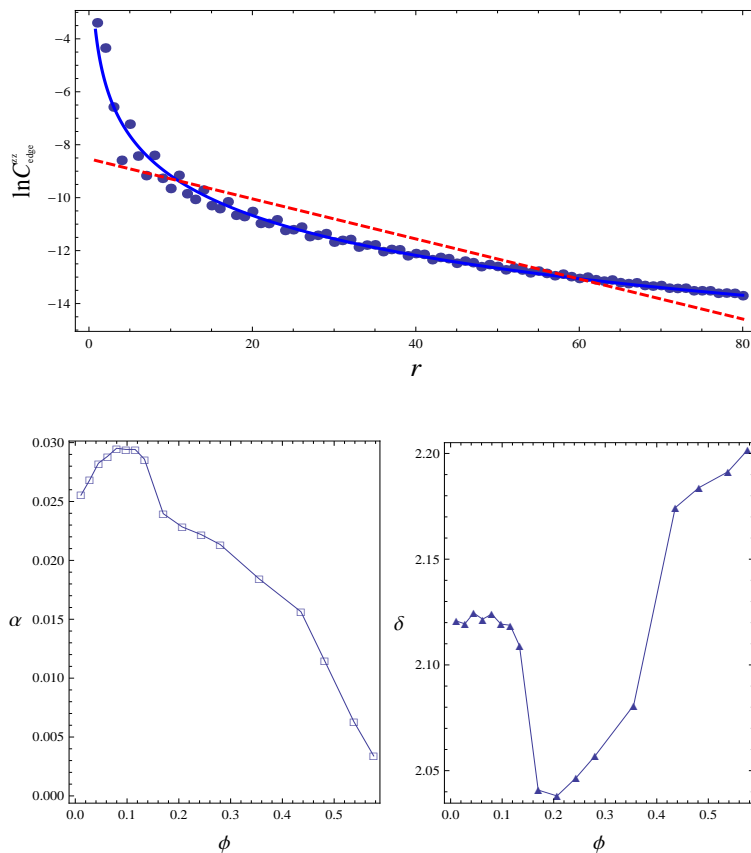


Figure 6. (Color online) (a) The spin correlation functions (in logarithm) along the right edge of the ribbon. The dots are the numerical results. Here the width of the system is $L_{\text{max}} = 50$, the model parameter is $\phi = 0.435847$ and the gauge choice is $\Delta\eta = \pi/2$. The solid blue line is a power-law fit ($\alpha \approx 0.0156407$ and $\delta \approx 2.174343$). The red dashed straight line is an exponential law fit. (b) The fitted coefficient α as a function of ϕ . (c) The fitted exponent δ as a function of ϕ . Please see more details in the text.

5. Summary

In a brief summary, we showed a possible gapped chiral spin liquid in the 2D square bilinear-biquadratic system in the region of $0 < \phi < \pi/4$. As a consequence, the time-reversal symmetry breaks spontaneously and an interesting topological ground state is revealed. We numerically analysed the resulting spin edge states for a ribbon system in detail. This method may be applied to other relating systems to specify a spin liquid state. We found \mathcal{L} (left) and \mathcal{R} (right) chiral edge modes for nonzero longitudinal momentum $k_x \neq 0$ and a zero edge modes for $k_x = 0$. The power-law decay of the edge spin correlation function and the contribution of the nontrivial spin edge state to the specific heat at low temperatures are found. In the future work, the properties of low energy excitations would be of great interest.

Acknowledgement

The authors thanks Professor Shun-Qing Shen for fruitful discussions. This work was supported by SRF for ROCS SEM (20111139-10-2), the Chinese National Natural Science Foundation under Grant No.: 11074177, 11174035. This research was supported in part by the Project of Knowledge Innovation Program (PKIP) of Chinese Academy of Sciences, Grant No. KJCX2.YW.W10.

Appendix: Classification topological state by Z_2 topological invariants

For each flavor of fermions (omit the flavor index μ in Eq. (14)), the effective Hamiltonian is

$$H_{eff} = \frac{1}{2} \sum_{\mathbf{k}} \Phi^\dagger(\mathbf{k}) M(\mathbf{k}) \Phi(\mathbf{k}), \quad (68)$$

with $M(\mathbf{k})$ defined in Eq. (16). From the results in Ref.[38], the 2×2 Pauli matrices can be divided into two groups - even matrix σ_z and odd matrices, σ_x and σ_y . Because the coefficients of odd matrices are zero at four high symmetry points of square lattice in momentum space, we can only focus on the coefficients of even matrix, $d_z(\mathbf{k}) = \lambda - 2J_1F(\cos k_x + \cos k_y)$. The four Z_2 topological invariants are defined as

$$\zeta_{\mathbf{k}} = 1 - \Theta(d_z(\mathbf{k})), \quad (69)$$

where $\Theta(x) = 1$ if $x > 0$ and $\Theta(x) = 0$ if $x < 0$.

Hence, for points $(0, 0)$, $(0, \pi)$, $(\pi, 0)$, (π, π) , the four Z_2 topological invariants are explicitly given by

$$\begin{aligned} \zeta_{k=(0,0)} &= \Theta[\lambda - 4J_1F], \\ \zeta_{k=(0,\pi)} &= \Theta[\lambda], \\ \zeta_{k=(\pi,0)} &= \Theta[\lambda], \\ \zeta_{k=(\pi,\pi)} &= \Theta[\lambda + 2J_1F]. \end{aligned} \quad (70)$$

For $\mathbf{k}=(\pi, \pi)$, $k = (0, \pi)$, $k = (\pi, 0)$, we have a trivial result as

$$\zeta_{\mathbf{k}=(\pi,\pi)} = \zeta_{k=(0,\pi)} = \zeta_{k=(\pi,0)} = 0; \quad (71)$$

for $\mathbf{k}=(0, 0)$, we have

$$\zeta_{\mathbf{k}=(0,0)} = \Theta(\lambda - 4J_1F). \quad (72)$$

Thus we identify two distinct topological states: the topological state with trivial topological invariants

$$\zeta_{\mathbf{k}=(0,0)} = \zeta_{\mathbf{k}=(\pi,\pi)} = \zeta_{\mathbf{k}=(0,\pi)} = \zeta_{\mathbf{k}=(\pi,0)} = 0 \quad (73)$$

for $\lambda > 4J_1F$ and the topological state with nontrivial topological invariants

$$\zeta_{\mathbf{k}=(\pi,\pi)} = \zeta_{\mathbf{k}=(0,\pi)} = \zeta_{\mathbf{k}=(\pi,0)} = 0, \zeta_{\mathbf{k}=(0,0)} = 1 \quad (74)$$

for $\lambda < 4J_1F$. And in the topological spin liquid state in this paper, we find a special fermion parity pattern: even fermion parity at $\mathbf{k} = (\pi, \pi)$, $\mathbf{k} = (0, \pi)$, and $\mathbf{k} = (\pi, 0)$ and odd fermion parity at $\mathbf{k} = (0, 0)$.

References

- [1] P. W. Anderson, *Mater. Res. Bull.* **8**, 153 (1973).
- [2] P. W. Anderson, *Science* **235**, 1196 (1987).
- [3] P. A. Lee, *Science* **321**, 1306 (2008).
- [4] P. Fazekas and P. W. Anderson, *Philos. Mag.* **30**, 432 (1974).
- [5] K. V. Klitzing, G. Dorda, and M. Pepper, *Phys. Rev. Lett.* **45**, 494 (1980).
- [6] R. Prange and S. Girvin, *The Quantum Hall Effect* (Springer, New York, 1987); H. Aoki, *Rep. Progr. Phys.* **50** (1987) 655; G. Morandi, *Quantum Hall Effect* (Bibliopolis, Naples, 1988).
- [7] C. L. Kane and E. J. Mele, *Phys. Rev. Lett.* **95**, 146802 (2005); **95**, 226801 (2005).
- [8] B. A. Bernevig, T. L. Hui and S. C. Zhang, *Science* **314**, 1757 (2006).
- [9] F. D. M. Haldane, *Phys. Rev. Lett.* **61**, 2015 (1988).
- [10] X. G. Wen, *Quantum Field Theory of Many-Body Systems*, (Oxford Univ. Press, Oxford, 2004).
- [11] H. H. Chen and P. M. Levy, *Phys. Rev. B* **7**, 4267 (1973).
- [12] N. Papanicolaou, *Nucl. Phys. B* **305**, 367 (1988).
- [13] F. D. M. Haldane, *Phys. Lett.* **93A**, 464 (1983); *Phys. Rev. Lett.* **50**, 1153 (1983).
- [14] I. Affleck, T. Kennedy, E. H. Lieb, and H. Tasaki, *Phys. Rev. Lett.* **59**, 799 (1987); *Commun. Math. Phys.* **115**, 477 (1988).
- [15] G. Fáth and J. Sólyom, *Phys. Rev. B* **44**, 11836 (1991).
- [16] G. Fáth and A. Sütő, *Phys. Rev. B* **62**, 3778 (2000).
- [17] T. Xiang and G. A. Gehring, *Phys. Rev. B* **48**, 303 (1993).
- [18] A. Läuchli, G. Schmid, and S. Trebst, *Phys. Rev. B* **74**, 144426 (2006).
- [19] U. Schollwöck, T. Jolicoeur, and T. Garel, *Phys. Rev. B* **53**, 3304 (1996).
- [20] K. Rommelse and M. den Nijs, *Phys. Rev. Lett.* **59**, 2578 (1987).
- [21] T. Kennedy, *J. Phys. Condens. Matter* **2**, 5737 (1990).
- [22] S. R. White and D. A. Huse, *Phys. Rev. B* **48**, 3844 (1993).
- [23] E. Polizzi, F. Mila, and E. S. Sørensen, *Phys. Rev. B* **58**, 2407 (1998).
- [24] T. Murashima, K. Nomura, *Phys. Rev. B* **73**, 214431 (2006).
- [25] Z. -C. Gu, X. -G. Wen, *Phys. Rev. B* **80**, 155131 (2009).
- [26] H. Tsunetsugu and M. Arikawa, *J. Phys. Soc. Jpn.* **75**, 083701 (2006).
- [27] A. Läuchli, F. Mila, and K. Penc, *Phys. Rev. Lett.* **97**, 087205 (2006).
- [28] P. Li, G. M. Zhang, and S. -Q. Shen, *Phys. Rev. B* **75**, 104420 (2007).
- [29] H. H. Zhao, Cenke Xu, Q. N. Chen, Z. C. Wei, M. P. Qin, G. M. Zhang, and T. Xiang, *Phys. Rev. B* **85**, 134416 (2012).
- [30] T. A. Tóth, A. M. Läuchli, F. Mila, and K. Penc, *Phys. Rev. Lett.* **105**, 265301 (2010).
- [31] K. Harada and N. Kawashima, *J. Phys. Soc. Jpn.* **70**, 13 (2001); *Phys. Rev. B* **65**, 052403 (2002).
- [32] A. Y. Kitaev, *Phys. Usp.* **44**, 131 (2001).
- [33] B. Zhou and S.-Q. Shen, *PRB* **84**, 054532 (2011).
- [34] P. Li and S. -Q. Shen, *New J. Phys.* **6**, 160 (2004); *Phys. Lett. A* **373**, 3075 (2009).
- [35] Z. -X. Liu, Y. Zhou, and T. -K. Ng, *Phys. Rev. B* **82**, 144422 (2010).
- [36] N. Read and D. Green, *Phys. Rev. B* **61**, 10267 (2000).
- [37] A. C. Potter and P. A. Lee, *Phys. Rev. Lett.* **105**, 227003 (2010).
- [38] S. P. Kou and X. G. Wen, *Phys. Rev. B* **80**, 224406 (2009).
- [39] M. Cheng, K. Sun, V. Galitski, and S. Das Sarma, *Phys. Rev. B* **81**, 024504 (2010).